

1           **Formation, radiative forcing, and climatic effects of severe regional haze**

2           Yun Lin<sup>1,2\*</sup>, Yuan Wang<sup>3\*</sup>, Bowen Pan<sup>1,4</sup>, Jiayi Hu<sup>1,5</sup>, Song Guo<sup>6</sup>, Misti Levy Zamora<sup>1,7</sup>,  
3           Pengfei Tian<sup>1,8</sup>, Qiong Su<sup>9</sup>, Yuemeng Ji<sup>1,10</sup>, Jiayun Zhao<sup>11</sup>, Mario Gomez-Hernandez<sup>11</sup>, Min  
4           Hu<sup>6</sup>, Renyi Zhang<sup>1,11\*</sup>

5           <sup>1</sup>Department of Atmospheric Sciences, Texas A&M University, College Station, TX 77843,  
6           USA

7           <sup>2</sup>Joint Institute for Regional Earth System Science and Engineering (JIFRESSE), University  
8           of California at Los Angeles, Los Angeles, CA 90064

9           <sup>3</sup>Division of Geological and Planetary Sciences, California Institute of Technology,  
10           Pasadena, CA 91125, USA

11           <sup>4</sup>Department of Atmospheric Science, Colorado State University, Fort Collins, CO, 80521,  
12           USA

13           <sup>5</sup>Cooperative Institute for Mesoscale Meteorological Studies, NOAA/OAR National Severe  
14           Storms Laboratory, Norman, OK, USA

15           <sup>6</sup>State Key Joint Laboratory of Environmental Simulation and Pollution Control, College of  
16           Environmental Sciences and Engineering, Peking University, Beijing, 10087, P.R. China

17           <sup>7</sup>Department of Environmental Health and Engineering, Johns Hopkins Bloomberg School of  
18           Public Health, 615 N. Wolfe St., Baltimore, MD 21205, USA

19           <sup>8</sup>Key Laboratory for Semi-Arid Climate Change of the Ministry of Education, College of  
20           Atmospheric Sciences, Lanzhou University, Lanzhou 730000, P. R. China

21           <sup>9</sup>Water Management & Hydrological Science, Texas A&M University, College Station, TX  
22           77843, USA

23           <sup>10</sup>Guangzhou Key Laboratory of Environmental Catalysis and Pollution Control, School of  
24           Environmental Science and Engineering, Institute of Environmental Health and Pollution  
25           Control, Guangdong University of Technology, Guangzhou 510006, China

26           <sup>11</sup>Department of Chemistry, Texas A&M University, College Station, TX 77843, USA

27           \*Correspondence: [yunlin@ucla.edu](mailto:yunlin@ucla.edu); [Yuan.Wang@caltech.edu](mailto:Yuan.Wang@caltech.edu); [renyi-zhang@tamu.edu](mailto:renyi-zhang@tamu.edu)

29

30 **Abstract.** Severe regional haze events, which are characterized by exceedingly high levels of  
31 fine particulate matter (PM), occur frequently in many developing countries (such as China  
32 and India), with profound implications for human health, weather, and climate. The occurrence  
33 of the haze extremes involves a complex interplay between primary emissions, secondary  
34 formation, and conducive meteorological conditions, and the relative contributions of the  
35 various processes remains unclear. Here we investigated severe regional haze episodes in 2013  
36 over the Northern China Plain (NCP), by evaluating the PM production and the interactions  
37 between elevated PM and the planetary boundary layer (PBL). Analysis of the ground-based  
38 measurements and satellite observations of PM properties shows nearly synchronized temporal  
39 PM variations among the three megacities (Beijing, Baoding, and Shijiazhuang) in this region  
40 and a coincidence of the aerosol optical depth (AOD) hotspots with the three megacities during  
41 the polluted period. During the clean-to-hazy transition, the measured oxygenated organic  
42 aerosol concentration ([OOA]) well correlates with the odd-oxygen concentration ( $[O_x] = [O_3]$   
43  $+ [NO_2]$ ), and the mean [OOA]/ $[O_x]$  ratio in Beijing is much larger than those in other  
44 megacities (such as Mexico City and Houston), indicating highly efficient photochemical  
45 activity. Simulations using the Weather Research and Forecasting (WRF) model coupled with  
46 an explicit aerosol radiative module reveal that strong aerosol-PBL interaction during the  
47 polluted period results in a suppressed and stabilized PBL and elevated humidity, triggering a  
48 positive feedback to amplify the haze severity at the ground level. Model sensitivity study  
49 illustrates the importance of black carbon (BC) in the haze-PBL interaction and the aerosol  
50 regional climatic effect, contributing to more than 30% of the PBL collapse and about half of  
51 the positive radiative forcing on the top of the atmosphere. Overall, severe regional haze  
52 exhibits strong negative radiative forcing (cooling) of -63 to -88 W m<sup>-2</sup> at the surface and strong  
53 positive radiative forcing (warming) of 57 to 82 W m<sup>-2</sup> in the atmosphere, with a slightly  
54 negative net radiative forcing of about -6 W m<sup>-2</sup> on the top of the atmosphere. Our work

55 establishes a synthetic view for the dominant regional features during severe haze events,  
56 unraveling rapid *in-situ* PM production and inefficient transport, both of which are amplified  
57 by atmospheric stagnation. On the other hand, regional transport sufficiently disperses gaseous  
58 aerosol precursors (e.g., sulfur dioxide, nitrogen oxides, volatile organic compounds, and  
59 ammonia) during the clean period, which subsequently result in rapid *in-situ* PM production  
60 via photochemistry during the transition period and via multiphase chemistry during the  
61 polluted period. Our findings highlight the co-benefits for reduction in BC emissions, which  
62 not only improve local and regional air quality by minimizing air stagnation but also mitigate  
63 the global warming by alleviating the positive direct radiative forcing.

64

65

66

67 **1. Introduction**

68 Rapid economic growth and urbanization have caused frequent severe regional haze  
69 events associated with heavy pollution of particulate matter (PM) in many developing countries,  
70 including China and India (Bouarar et al., 2017; Molina, 2021). The severe haze events induce  
71 great degradation in visibility and air quality, with profound societal implications (An et al.,  
72 2019). For example, exposure to elevated levels of fine PM leads to adverse health effects,  
73 ranging from aggravated allergies to the development of chronic diseases, to premature death  
74 (Pope and Dockery, 2015; Wu et al., 2019; Rychlik et al., 2019; Johnson et al., 2021; Zhang et  
75 al., 2021). Also, elevated levels of fine aerosols result in pronounced modifications to clouds,  
76 precipitation, and lightning, impacting regional/global weather and climate (Zhang et al., 2007;  
77 Yuan et al., 2008; Qian et al., 2009; Wang et al., 2011; Wang et al., 2014; Wu et al., 2016).  
78 Specifically, by absorbing/scattering solar radiation, aerosols impact the atmospheric stability  
79 and the energy budget of Earth, via the aerosol-radiation interaction (ARI). By serving as cloud  
80 condensation nuclei (CCN) and ice nucleating particles (INPs), aerosols influence the macro-  
81 and microphysical properties of clouds, via the aerosol–cloud interaction (ACI). Currently, the  
82 radiative forcing associated with ARI and ACI represents the largest uncertainty in the  
83 projection of future climate by anthropogenic activities (IPCC, 2013).

84 PM is either emitted directly into the atmosphere (primary) or produced in air via gas-  
85 to-particle conversion (secondary) (Zhang et al., 2015a). In addition, primary and secondary  
86 PM undergo chemical and physical transformations and are subjected to cloud processing and  
87 removal from air (Zhang et al., 2015a). Direct emissions of primary gases and PM and highly  
88 efficient secondary PM formation represent the primary processes leading to severe haze (Guo  
89 et al., 2014; Sun et al., 2014; Wang et al., 2016a; Peng et al., 2021). In addition, conducive  
90 weather conditions for pollutant accumulation, such as regional control by high-pressure,  
91 suppressed local circulations, and weakened large-scale circulation, correspond to the external

92 causes for severe haze formation (Liu et al., 2013; Wang et al., 2014d; Cai et al., 2017; Li et  
93 al., 2019).

94 The key constituents of fine PM include secondary inorganic (including sulfate, nitrate,  
95 and ammonium) aerosol (SIA) and secondary organic aerosol (SOA), with the corresponding  
96 gaseous precursors of sulfur dioxide (SO<sub>2</sub>), nitrogen oxides (NO<sub>x</sub> = NO + NO<sub>2</sub>), ammonia  
97 (NH<sub>3</sub>), and volatile organic compounds (VOCs). The photochemistry represents one of the  
98 mechanisms leading to SIA and SOA accumulation during the early stage of haze evolution  
99 (Guo et al., 2014; Zhang et al., 2015a; Wang et al., 2016; Zhang et al., 2020). Field  
100 measurements have shown that remarkably nucleation and growth of nanoparticles are  
101 primarily driven by photochemical activity, which is characterized by elevated ozone levels  
102 and efficient photolysis rate coefficients under clean daytime conditions (Zhang et al., 2015b;  
103 Guo et al., 2020). During haze evolution, the photochemical activity is typically reduced, as  
104 evident by low levels of ozone and reduced photolysis rates (Peng et al., 2021). On the other  
105 hand, there are increasing air stagnation and relative humidity (RH), when explosive secondary  
106 aerosol formation occurs (Peng et al., 2021). The latter has been attributed the occurrence of  
107 multiphase chemistry, which largely drives the formation of SIA and SOA during the polluted  
108 period (Peng et al., 2021). Currently, the relative contributions of primary emissions, secondary  
109 production, and regional transport to severe haze formation remain uncertain (Li et al., 2015;  
110 Zhang et al., 2015b; Peng et al., 2021). Moreover, the efficiency of photochemical PM  
111 production during regional haze events in NCP and its distinction among various megacities  
112 worldwide remain to be quantified (Molina, 2021).

113 While the importance of regional haze on climate has been recognized (Ramanathan et  
114 al., 2007; Wang et al., 2009; Wang et al., 2015a), there still lacks quantification for the aerosol  
115 radiative forcing and the climatic effects for severe regional haze events. Estimation of the  
116 aerosol radiative forcing during severe haze events exhibits a large variation (Li et al., 2007;

117 Xia et al., 2007; Wang et al., 2009; Che et al., 2014). In addition, the interactions between  
118 aerosols and planetary boundary layer (PBL) via the aerosol radiative effects likely increase  
119 the haze severity (Wang et al., 2015a; Wang et al., 2016b; Zhang et al., 2018). Meteorological  
120 conditions within the PBL, including the atmospheric stability and RH, are altered by the  
121 aerosol-PBL interaction to induce a positive feedback to PM accumulation near the ground  
122 level (Tang et al., 2016a; Tie et al., 2017; Wu et al., 2020). However, the aerosol-PBL  
123 interactions and their feedbacks to atmospheric thermodynamics and dynamics under  
124 extremely hazy conditions remain to be quantified (Li et al., 2017).

125 Previous studies have documented the role of black carbon (BC) in the aerosol-PBL  
126 interactions and the aerosol regional climate effects (Menon et al., 2002; Bond et al., 2013;  
127 Wang et al., 2013; Ding et al., 2016). In addition, the BC aging process markedly enhances BC  
128 absorption by modifying the particle physiochemical and optical properties (Zhang et al., 2008;  
129 Khalizov et al., 2013; He et al., 2015; Guo et al., 2016; Peng et al., 2016; Peng et al., 2017).  
130 For example, an experimental/field study showed that the mass absorption cross section (MAC)  
131 of BC is enhanced by 2.4 times in a short time because of BC aging under polluted urban  
132 conditions (Peng et al., 2016), reconciling previous variable results on the coating-enhanced  
133 absorption for BC (Gustafsson and Ramanathan, 2016). Apparently, the enhancement of the  
134 BC absorption causes additional aerosol radiative forcing (Peng et al., 2016) and suppression  
135 on PBL development (Wang et al., 2017). Currently, limited modeling studies have assessed  
136 the radiative effect of BC aging associated with severe regional haze (Wang et al., 2013; He et  
137 al., 2015; Gustafsson and Ramanathan, 2016).

138 To better understand the formation and evolution of severe regional haze as well as  
139 their regional and climate effects, we investigated severe haze episodes occurring in 2013 over  
140 the Northern China Plain (NCP). The NCP region, which encompasses the megacities of  
141 Beijing and Tianjin, and some portion of the provinces of Heibei, Shandong, and Henan,

142 represents the most polluted area in China (An et al., 2019). Satellite observations and field  
143 measurements of PM properties were evaluated, and numerical simulations were performed to  
144 elucidate the interactions between severe haze and PBL using Weather Research and Forecast  
145 (WRF) model coupled with an explicit aerosol radiative module (Fan et al., 2008; Wang et al.,  
146 2014c). By conducting model sensitivity simulations, we elucidated the impacts of BC aging  
147 on the haze-PBL interactions and its contribution to the net aerosol radiative forcing during  
148 severe haze periods.

## 149 **2. Methodology**

150 The NCP represents a key economic zone in China, as reflected by its gross domestic  
151 product (GDP), energy consumption, and vehicular fleets (An et al., 2019). The region has  
152 undergone fast industrialization and urbanization over the past four decades. For example, NCP  
153 is one of the most densely populated regions in the world and contributes to over 1/10 of the  
154 GDP in China. The consumption of coal and crude oil in NCP was 363 and 72 million tons,  
155 respectively, to 1,348 million tons in 1998 and increased to 140 million tons of standard coal  
156 equivalent in 2010, respectively. In particular, anthropogenic activities result in industrial,  
157 traffic, residential, and agricultural emissions, representing the major sources for PM  
158 precursors, including SO<sub>2</sub>, NO<sub>x</sub>, VOCs, and NH<sub>3</sub> (An et al., 2019; Peng et al., 2021).  
159 Surrounded by the Taihang Mountains to the west and Yanshan Mountains to the north,  
160 respectively, the NCP region is prone to develop air stagnation under conducive meteorological  
161 conditions, inhibiting vertical and horizontal dispersion of air pollutants (An et al., 2019; Peng  
162 et al., 2021).

### 163 **2.1. The Data Sources**

164 The satellite-retrieved aerosol optical depth (AOD) was derived by combining the  
165 Moderate Resolution Imaging Spectroradiometer (MODIS) measurements of Aqua and Terra  
166 using the equal-weighted mean method to increase the spatial coverage (Levy et al., 2009). The

167 MODIS data are accessible at <http://giovanni.gsfc.nasa.gov/aerostat/>. The Terra visible images  
168 were obtained at <https://worldview.earthdata.nasa.gov/>. The hourly PBL height used was based  
169 on the Modern-Era Retrospective analysis for Research and Applications, Version 2 (MERRA2)  
170 reanalysis data. The severe haze days were selected with daily PM<sub>2.5</sub> (particular matter with  
171 aerodynamic diameter less than 2.5 micron) concentration greater than 200  $\mu\text{g m}^{-3}$ , and the  
172 typical clean days were limited to the days with daily PM<sub>2.5</sub> concentration smaller than 30  $\mu\text{g}$   
173  $\text{m}^{-3}$ . The PBL height and the PM<sub>2.5</sub> surface concentration at 14:00 Beijing time (BJT) each day  
174 in 2013 were used for the correlation analysis. All raining days were filtered out when  
175 analyzing the correlation between the PBL height and the PM<sub>2.5</sub> concentration. The surface  
176 solar radiation (SSR) data were based on the satellite retrievals (Tang et al., 2016b), which are  
177 accessible at <http://www.tpdatabase.cn>.

178 Ground-based measurements of fine particulate matter or PM<sub>2.5</sub> employed in our  
179 analysis covered the period from 25 September to 14 November 2013. The hourly PM<sub>2.5</sub>  
180 concentrations in Beijing (BJ) were obtained from the Embassy of United States in Beijing  
181 (<http://www.stateair.net/web/historical/1/1.html>). The PM<sub>2.5</sub> mass concentrations in Baoding  
182 (BD) and Shijiazhuang (SJZ) were obtained from <https://air.cnemc.cn:18007/>. Measurements  
183 of PM properties in Beijing were taken from that previously reported by Guo et al. (2014),  
184 which provided PM<sub>2.5</sub> concentration, aerosol chemical composition, and gaseous data for  
185 correlation analysis and constrains for modeling studies. For example, the mass concentrations  
186 of various inorganic and organic aerosol species, including oxygenated organic aerosol (OOA),  
187 were measured using an aerosol mass spectrometer (AMS) in Beijing (Aiken et al., 2009; Guo  
188 et al., 2014). The observation-based analysis and the modeling study focused on two severe  
189 haze episodes, i.e., 25 September – 30 September (episode 1 or EP1) and 2 October – 6 October  
190 (episode 2 or EP2), 2013 in NCP.



191 **2.2. Model experiments**

192 **2.2.1. Simulations on the haze-PBL interactions**

193 The aerosol-PBL interactions during the severe haze events and the associated regional  
194 climate effects were examined by conducting WRF modeling sensitivity studies. An aerosol  
195 radiative module was implemented by Fan et al. (2008) to the Goddard Shortwave Radiation  
196 Scheme to online compute the wavelength-dependent aerosol optical properties, including the  
197 AOD, the asymmetry factor and the single scattering albedo (SSAs). Aerosol particles with the  
198 core-shell configuration in the aerosol radiative module were assumed to consist of BC (core)  
199 and ammonia sulfate (shell). The hygroscopic growth of aerosol particles was taken into  
200 account, following Mallet et al. (2004). A two-moment bulk microphysical scheme developed  
201 by Li et al. (2008) was employed, which has been widely used to investigate the aerosol-cloud  
202 interactions under various cloud systems (Wang et al., 2014b; Wang et al., 2014a; Lin et al.,  
203 2016). A 100×100 grids domain with a horizontal grid spacing of 2 km and 50 vertical levels  
204 with stretched grid spacings was set up to cover the entire urban region of Beijing. The initial  
205 and boundary meteorological conditions were generated from six-hourly NCEP FNL (Final)  
206 Operational Global Analysis (1°×1°). No convective parametrization was applied for the  
207 simulations.

208 We performed simulations on the two haze episodes (EP1 and EP2). The two days prior  
209 to the two haze episodes (25 September and 2 October, 2013) are denoted as the clean periods,  
210 while the most polluted days during the two episodes, i.e., 28 September and 5 October are  
211 denoted as the polluted periods. The aerosol number size distributions for initial and boundary  
212 conditions of all simulation were based on the measurements during the 2013 field campaign  
213 at Beijing (Fig. S1). The aerosol measurements on 25 September and 2 October 2013 were  
214 taken as the input for the clean cases and 28 September and 5 October 2013 for the polluted  
215 cases. The aerosol surface number and mass concentration for modeling initialization were set

216 as  $3.5 \times 10^4 \text{ cm}^{-3}$  ( $3.6 \times 10^4 \text{ cm}^{-3}$ ) and  $10 \text{ } \mu\text{g m}^{-3}$  ( $11 \text{ } \mu\text{g m}^{-3}$ ) for the clean case of EP1 (EP2) and  
217  $1.7 \times 10^4 \text{ cm}^{-3}$  ( $1.8 \times 10^4 \text{ cm}^{-3}$ ) and  $280 \text{ } \mu\text{g m}^{-3}$  ( $310 \text{ } \mu\text{g m}^{-3}$ ) for the polluted case of EP1 (EP2),  
218 respectively, consistent with the field measurements. Also, based on the measurements, the BC  
219 percentage in total aerosol mass was set as 10.0% and 6.0% for the clean and polluted cases,  
220 respectively. The two polluted days for simulations were cloud-free days, therefore the aerosol  
221 indirect effects were ruled out.

222 To assess the role of BC in the aerosol suppression effect on the PBL development and  
223 the aerosol radiative forcing during haze evolution, we performed a set of sensitivity  
224 simulations under the polluted condition by excluding the BC effects (referred as non-BC case),  
225 in which the BC radiative effect was turned off by assigning a zero value to the real and  
226 imaginary parts of BC refractive index, i.e., the SSA in non-BC case was equal to unity. To  
227 quantify the BC aging effects, additional simulations were carried out for fresh BC (denoted  
228 by fresh-BC), in which the BC core was not imbedded in the non-BC shell and the optical  
229 parameters for the BC and non-BC components were calculated separately by the Mie theory.  
230 In the fresh-BC case, the lensing effect due to the coating during the aging process was  
231 excluded, but the restructuring effect induced by aging was considered partially since the BC  
232 core was assumed to be spherical and in the compact shape. Alternatively, a case for aged BC  
233 (denoted by aged-BC) was treated by considering the full aerosol components (with both BC  
234 and non-BC components) and the core-shell configuration. A summary of the simulation cases  
235 is listed in Table 1.

236 One deficiency to predict the absorbed AOD and the directive radiation forcing of BC  
237 in atmospheric models is relevant to the underestimation in coating-enhancement of BC  
238 absorption (Bond et al., 2013). To assess the potential bias on the radiative effects of aged BC,  
239 additional simulations on the polluted conditions were conducted by constraining the  
240 enhancement of mass absorption cross section of BC ( $E_{\text{MAC-BC}}$ ) according to the experimental

241 value, i.e., 2.4, derived from a chamber study in Beijing (Peng et al., 2016). Though the  $E_{MAC-}$   
242  $_{BC}$  of 2.3 derived from the aged-BC case is slightly lower than that reported by Peng et al.  
243 (2016), comparison between the two simulations indicates little difference in the  
244 thermodynamic/dynamic conditions and the radiative budget.

### 245 **2.2.2. Empirical estimation of the moisture effect on haze-PBL interactions**

246 In addition to the numerical model simulations, we employed an empirical equation  
247 derived by Nozaki (1973) and modified by Tie et al. (2017) to examine the RH sensitivity in  
248 the boundary layer to the PBL height based on observed meteorological conditions:

$$249 \quad H = \frac{121}{6} (6 - P)(T - T_d) + \frac{0.169P(U_z + 0.257)}{12f \ln Z/z_0} \quad (1)$$

250 where  $H$ ,  $T$ ,  $T_d$ , and  $U_z$  represent the PBL height (m), surface air temperature (K), surface dew  
251 point (K), and mean wind speed ( $\text{m s}^{-1}$ ) at height of  $Z$  ( $Z=10$  m), respectively.  $f$  and  $z_0$  are the  
252 Coriolis parameter ( $\text{s}^{-1}$ ) and surface roughness length (0.5 m in this study), respectively.  $P$  is  
253 the Pasquill stability level, classified as six categories from very unstable (A), moderately  
254 unstable (B), slightly unstable (C), neutral (D), slightly stable (E) to moderately stable (F)  
255 (Pasquill, 1961). To relate RH with the PBL height, we adopted a modified Nozaki's equation  
256 using  $(100 - \text{RH})/5$  to replace  $(T - T_d)$  according to Wallace and Hobbs (2005) and Tie et al.  
257 (2017). The measured wind speeds were used in the calculations. For the severe haze events,  
258 the atmosphere was stable, and the Pasquill stability levels were set as 4~5. The input of the  
259 PBL height for the aged-BC cases were based on ceilometer measurements, and we increased  
260 the PBL height by about 1000 m as the input for the clean cases, which was estimated based  
261 on MERRA2 reanalysis data due to the lack of relevant measurements.

## 262 3. Results and Discussion

### 263 3.1. Regional characteristics of severe haze episodes

264 Measurements of the PM<sub>2.5</sub> mass concentrations from 25 September to 14 November  
265 2013 reveal that severe haze occurs frequently over the NCP, reflected by a periodic cycle of  
266 4-7 days with highly elevated PM pollution (Fig. 1a-c). Each severe haze episode consists of a  
267 clean period, a transition period from clean to hazy conditions, and a polluted period with very  
268 high PM levels. For the three megacities across the NCP, i.e., Beijing, Baoding, and  
269 Shijiazhuang, the maximal mass concentration of PM<sub>2.5</sub> consistently exceed several hundred  
270  $\mu\text{g m}^{-3}$  during the polluted period. The PM<sub>2.5</sub> concentrations at the three megacities exhibit a  
271 remarkable similarity in the timing and magnitude for the peak PM<sub>2.5</sub> concentrations. The  
272 nearly synchronized temporal variations in the PM levels among the three megacities indicate  
273 a prominent characteristic of severe haze formation, indicating the importance of *in-situ* PM  
274 production over the entire region. During the evolution from clean, transition, to polluted  
275 periods, the RH and wind speed is consistently increased and decreased, respectively (Fig. 1d).

276 The two polluted events on 28 September (EP1) and 5 October (EP2) are captured from  
277 both *in-situ* measurements (Fig. 1) and satellite observations (Fig. 2). The satellite MODIS data  
278 illustrate that the maximal AOD area occurs in the three megacities (i.e., BJ, BD, and SJZ). For  
279 example, the AOD value in Beijing exceeds 4.0 and 2.0, during EP1 and EP2, respectively.  
280 The spatial distribution of severe regional haze events is also depicted from the satellite visible  
281 images, showing that a grey haze plume covers a substantial portion of the NCP region (Figs.  
282 2c and d). The coincidence of the highest AOD areas with the locations of the megacities is  
283 also discernable from the mean AOD values averaged over all the hazy days (e.g., daily PM<sub>2.5</sub> >  
284 200  $\mu\text{g m}^{-3}$ ) in 2013 (Fig. S3), showing a large zone of elevated AOD values over the three  
285 megacities. In contrast, the fall seasonal and annual AOD means averaged over all days in 2013  
286 show that the maximal AOD values are located to the south of Beijing (Figs. 2e and f),

287 reflecting the typical regional transport patterns over this region (Guo et al., 2014; An et al., 2019;  
288 Peng et al., 2021). In addition, the occurrence of severe haze events is consistently  
289 accompanied by stagnant weather, characterized by weak southerly winds in Beijing and its  
290 surrounding areas (Figs. 2a and b). For example, the wind speed is typically less than  $1 \text{ m s}^{-1}$   
291 in the highest AOD area (Figs. 2a and b), compared to that of a few to ten  $\text{m s}^{-1}$  during the clean  
292 period (Fig. 1d). Air stagnation retards PM dispersion, resulting in minimal regional transport  
293 during the polluted period. On the other hand, the gaseous aerosol precursors (e.g.,  $\text{SO}_2$ ,  $\text{NO}_x$ ,  
294 VOCs, and  $\text{NH}_3$  with the chemical lifetimes from hours to days) are sufficiently transported  
295 and dispersed prior to haze development over this region, as evident from much higher wind  
296 speeds during the clean period (Fig. 1d). Efficient regional transport of the gaseous aerosol  
297 precursors explains the similarity in the spatial/temporal PM variations, since well-mixed  
298 gaseous aerosol precursors result in similar *in-situ* PM production under stagnant conditions  
299 (Figs. 1a-c). Moreover, the coincidence of the AOD hotspots with the three megacities (Figs.  
300 2a, b and S3) indicates more efficient *in-situ* PM production over the megacities, suggesting a  
301 key role of traffic emissions (i.e., anthropogenic VOCs and  $\text{NO}_x$ ) in facilitating regional severe  
302 haze formation. While wind fluctuation likely results in PM variation in an isolated location,  
303 especially for Beijing, which is situated at the northern edge of the NCP (Li et al., 2015), our  
304 analysis of temporal/spatial PM distributions indicates that the dominant regional features  
305 during the polluted period are reflected by rapid *in-situ* PM production and inefficient transport,  
306 both of which are amplified by air stabilization.

### 307 3.2. Photochemical PM formation

308 To further elucidate the role of *in-situ* photochemical production in haze development,  
309 we analyzed the temporally resolved PM properties in Beijing. Evidently, the  $\text{PM}_{2.5}$  mass  
310 concentration increases by more than  $200 \mu\text{g m}^{-3}$  in less than 8 hrs. during the transition period  
311 for EP1 and EP2 (Figs. 3a and b), which is dominated by the increase in the SOA mass

Deleted: (

313 concentration linked to photochemical oxidation of VOCs (Guo et al., 2014; Liu et al., 2021).  
314 The mass concentration of OOA is typically considered as a surrogate for SOA (Wood et al.,  
315 2010). Since OOA and the level of oxidants,  $O_x$  ( $[O_x] \equiv [O_3] + [NO_2]$ ), are both produced  
316 from oxidation of VOCs (Suh et al., 2001; Fan and Zhang, 2004; Zhao et al., 2004, 2005) and  
317 have a lifetime of longer than 12 hours, it is anticipated that both quantities are correlated, when  
318 their formations occur on a similar timescale and at the same location (Atkinson, 2000). Figs.  
319 3a-d show that the increase in OOA is well correlated with the  $O_x$  level during the transition  
320 period. The  $R^2$  from linear regression between OOA and  $O_x$  during the transition period (i.e.,  
321 from 7:00 am to 2:30 pm) is 0.96 for EP1 and 0.95 for EP2 (Fig. 3e). The high correlation  
322 between OOA and  $O_x$  implies important *in-situ* production of PM via photochemical reactions,  
323 consistent with the ground-based measurements (Fig. 1) and satellite observations for PM (Fig.  
324 2 and Fig. S3). The mean ratio of [OOA] to [ $O_x$ ] for the two episodes in Beijing is 0.34 ( $\mu\text{g m}^{-3}$   
325  $\text{ppb}^{-1}$ ), suggesting highly efficient photochemistry. For comparison, the mean ratio of [OOA]  
326 to [ $O_x$ ] during the two episodes in Beijing is about 2.4 and 5.1 times of those in Mexico City  
327 and Houston (Wood et al., 2010), respectively, indicating that the photochemical PM formation  
328 in Beijing is much more efficient than those in Mexico City and Houston (Fig. 3f). The more  
329 efficient photochemical formation of PM in Beijing is attributable to the presence of higher  
330 levels of anthropogenic aerosol precursors, such as anthropogenic VOCs and  $NO_x$ , than those  
331 in the other two cities (Guo et al., 2014; Zhang et al., 2015a). On the other hand, the correlation  
332 between [OOA] and [ $O_x$ ] exists only during the transition stage but vanishes during the polluted  
333 period. The latter is evident from the continuing increase in [OOA] but decreasing [ $O_x$ ]. In  
334 particular,  $O_3$  production is significantly suppressed during the polluted periods because of  
335 reduced solar ultraviolet radiation, leading to inefficient photooxidation (Wu et al., 2020; Peng  
336 et al., 2021). Several previous studies have attributed highly elevated levels of  $PM_{2.5}$  during the  
337 polluted period to the importance of multiphase chemistry to contribute to SIA and SOA

Deleted: oxygenated organic aerosol (

Deleted: )

340 formation (Wang et al., 2016; An et al., 2019; Peng et al., 2021). For example, sulfate formation  
341 is effectively catalyzed by BC (Zhang et al., 2020) and considerably enhanced via aqueous  
342 oxidation of SO<sub>2</sub> by NO<sub>2</sub> in the presence of NH<sub>3</sub> during the transition/polluted periods (Wang  
343 et al., 2016), both increasing with increasing RH. Also, oligomerization from dicarbonyls  
344 increases at high RH (Li et al., 2021a, b), contributing to significantly enhanced SOA formation  
345 during the polluted periods (Zhang et al., 2021).

346 Note that both the photochemical formation during daytime and the collapse of  
347 boundary layer in late afternoon can contribute to the pollution development. Since the PBL  
348 heights on the two transition days show an increase from morning to afternoon and a decrease  
349 from afternoon to midnight (Fig. S4), it is likely that the photochemical production of PM  
350 caused more pollution from morning to afternoon than did the collapse of boundary layer in  
351 the late afternoon. This is because the PM pollution produced by photochemistry could be  
352 diluted as the PBL developed.

### 353 **3.3. Impacts of the haze-PBL interaction**

#### 354 **3.3.1. A positive feedback of PM accumulation**

355 To assess the impacts of haze-PBL interactions on PM pollution, we evaluated the  
356 correlation between the PM level and PBL height. Fig. 4 shows an analysis of daily PBL height  
357 versus PM<sub>2.5</sub> concentration between clean and hazy days from the ground-based measurements  
358 and the MERRA2 reanalysis data in 2013. The daily PBL height is negatively correlated with  
359 surface PM<sub>2.5</sub> concentration (Fig. 4a). The diurnal cycle of the PBL height shows that the PBL  
360 height on severe haze days (daily PM<sub>2.5</sub> concentration > 200 µg m<sup>-3</sup>) is significantly lower than  
361 that on clean days (daily PM<sub>2.5</sub> concentration < 30 µg m<sup>-3</sup>), with a maximum difference of 800  
362 m (Fig. 4b). Furthermore, the dimming area over NCP, which is reflected by the lower mean  
363 of the satellite-retrieved surface solar radiation (SSR) averaged over all the severe haze days  
364 in 2013, coincides with the region with the highest AOD (Fig. S3), implying a strong spatial

365 association between the solar radiation intensity and PM pollution at the surface. The co-  
366 locations in the areas between the lowest SSR and highest AOD also reflects the occurrence of  
367 the highest PM levels at the megacities during the regional severe haze episodes.

368 We further elucidated the response of PBL development to the PM pollution, and the  
369 linkage between the aerosol-PBL interactions and aerosol radiative effects are further  
370 elucidated by performing sensitivity modeling studies on the two hazy days (Figs. 5-6). The  
371 performance of the model simulations was validated by comparison with field observations.  
372 The simulated temperature and RH are consistent with the sounding data in light of the vertical  
373 variations (Fig. S2). The simulated AOD at 550 nm is 0.05 and 3.6 on 25 and 28 September  
374 2013 for EP1, respectively, and 0.04 and 2.0 on 2 and 5 October 2013 for EP2, respectively, in  
375 qualitative agreement with the Aerosol Robotic Network (AERONET) measurements in  
376 Beijing (Table 2). The simulated one-day accumulated surface solar radiation and the peak  
377 solar radiation flux in the aged-BC case for EP1 (EP2) are  $9.2 \text{ MJ m}^{-2}$  ( $11.3 \text{ MJ m}^{-2}$ ) and  $326$   
378  $\text{W m}^{-2}$  ( $402 \text{ W m}^{-2}$ ), respectively, comparable to the ground-based measurement of  $10.6 \text{ MJ m}^{-2}$   
379 ( $9.8 \text{ MJ m}^{-2}$ ) and  $408 \text{ W m}^{-2}$  ( $452 \text{ W m}^{-2}$ ) in Table 2. The temporal evolutions of PBL and its  
380 peak heights derived from the aged-BC cases are also consistent with the available  
381 measurements (Figs. 5a and g).

382 The simulated maximal height of PBL under the polluted condition is reduced by more  
383 than 300 m relative to the clean condition (Figs. 5a and g). The reduction in PBL height is  
384 explained by the aerosol radiative effects. Under the polluted condition, a warmer temperature  
385 is located at the altitude of around 1.2 km, and less SSR reaches the ground level (Figs. 5e and  
386 k, f and l). Also, the surface temperature is reduced by several degrees (Figs. 5e and k, and  
387 Figs. 6a and c). Consequently, the turbulent kinetic energy (TKE) is reduced, and the updraft  
388 is weakened in the aged-BC cases relative to the clean cases (Figs. 5b, c, h and i), leading to an  
389 enhanced atmospheric stratification and hindered development of PBL. The largely reduced



390 TKE during the polluted periods from the model simulations is consistent with field  
391 measurements, showing that the turbulent fluxes are greatly reduced in the mixed surface layer  
392 under polluted conditions (Wilcox et al., 2016). In addition, surface winds are reduced by 0.7  
393  $\text{m s}^{-1}$  from clean to aged-BC cases (Fig. 6b and d), leading to suppressed entrainment aloft and  
394 restricted development of the PBL.

395 The interaction between aerosols and PBL induces further feedbacks at the surface by  
396 altering atmospheric dynamic/thermodynamic conditions and stability. For example, the PM  
397 concentration at the ground level accumulates when the PBL is compressed, resulting in a  
398 smaller extent for vertical dilution. Also, the diurnal feature of PM pollution diminishes  
399 because of collapsed PBL, allowing PM to continuously accumulate at the surface. In addition,  
400 horizontal advection is also suppressed under polluted conditions, as reflected by weak wind  
401 speeds. Consequently, the heavy haze period persists over an extensive period (about 4-7 days)  
402 over this region and is only dissipated by strongly northerly winds associated with frontal passage  
403 (Guo et al., 2014; An et al., 2019). The continuous PM accumulation for multiple days over  
404 the NCP is distinct from other megacities across the world, such as Houston, Los Angeles, and  
405 Mexico City, which always exhibit a clear diurnal feature of the PM levels (Zhang et al., 2015a),  
406 implying a key role of the haze-PBL interaction in deteriorating air quality and worsening the  
407 hazy condition in this region.

408 The suppression in PBL height results in significant enhancement of atmospheric  
409 moisture, another crucial factor affects the haze evolution, which promotes the occurrence of  
410 multiphase reactions (Li et al., 2021a, b). The measured RH increases greatly during the two  
411 episodes (Fig. 1d), i.e., from about 18%-19% on the clean days (25 September and 2 October)  
412 to 53%-55% on the polluted days (28 September and 5 October). To evaluate the sensitivity of  
413 the atmospheric moisture to the PBL height, we employed a modified Nozaki's equation  
414 (Nozaki, 1973; Tie et al., 2017) to calculate the RH under different PBL height scenarios using

415 the observed meteorological conditions as inputs (Table 3). The calculated RH increases from  
416 29% to 68% for EP1 and from 28% to 73% for EP2, when the PBL height decreased from 1180  
417 to 395 m and 1313 to 370 m from clean days to the polluted days for EP1 and EP2, respectively,  
418 indicating that the humidity is highly sensitive to the PBL height.

419 The elevated RH during the polluted period is explained from collapsed PBL to inhibit  
420 vertical moisture transport, reduced surface temperature leading to lower saturation vapor  
421 pressure, and inefficient entrainment of dry air aloft (Fan et al., 2008; Liu et al., 2013). In  
422 addition, enhanced moisture leads to hygroscopic growth of aerosol particles (Liu et al., 2013;  
423 Tie et al., 2017). For example, the growth hygroscopic factor relevant to the RH enhancement  
424 during EP1 and EP2 increases from 1.3 on the clean days to 1.5 on the hazy days, using an  
425 empirical equation derived according to Meier et al. (2009). The additional aerosol growth  
426 causes additional attenuation of incoming solar radiation by scattering and absorption to  
427 amplify PBL suppression. Moreover, an enlarged aerosol surface area (due to hygroscopic  
428 growth) and elevated RH during the polluted periods favor aqueous-phase reactions to produce  
429 sulfate, nitrate, and SOA (Wang et al., 2016a). For example, a recent experimental/field study  
430 has shown enhanced sulfate formation, which is catalyzed by BC and increases monotonically  
431 from 10% to 70% RH (Zhang et al., 2020). Also, the aqueous reaction of dicarbonyls, which  
432 are produced with high yields from oxidation of aromatic VOCs, is significantly enhanced at  
433 high RH to yield oligemic products and enhance SOA formation (Li et al., 2021a; b). Hence,  
434 enhanced PM production near the ground level strengthens the suppressing effect for the PBL  
435 development and results in stabilization and moisture enhancement, constituting positive  
436 feedback to amplify the haze development.

### 437 3.3.3. The BC effects

438 We performed model sensitivity simulations to elucidate the role of BC in PBL  
439 suppression by considering the non-BC, fresh-BC, and aged-BC scenarios during the polluted

Deleted: 1  
Deleted: 1  
Deleted: by about 1000 m during

443 periods. Comparison shows a negligible effect on the haze-PBL interaction between the non-  
444 BC and fresh-BC cases (Figs. 5, 6 and S5) but large changes in solar radiation and  
445 thermodynamic/dynamic conditions within the PBL between the non-BC/ fresh-BC and aged-  
446 BC cases, which are attributed to the radiative effects of aged BC. For example, the shortwave  
447 heating rate per unit mass is much larger for aged-BC than non-BC and is two times higher for  
448 aged-BC than fresh-BC (Figs. 5d and j), suggesting that the BC aging process greatly attenuate  
449 incoming solar radiation. Although BC accounts for only 6% of the total aerosol mass under  
450 the polluted conditions, about one third of the total reduction in SSR for full-component  
451 aerosols is attributed to absorption enhancement after BC aging (Figs. 5f and l). The reduced  
452 SSR by the BC aging leads to a cooling of 0.5-0.8 K at the surface. As a result, BC aging  
453 contributes significantly to atmospheric stabilization, as evident from weaker updrafts, smaller  
454 TKE, and shallower PBL for the aged-BC case (Fig. 5).

455 The BC aging causes a decrease in the maximum PBL height (at noontime) by about  
456 150 m for the aged-BC case compared to the non-BC and fresh-BC cases. Overall, the BC  
457 aging contributes more than 30% of the total reduction in the PBL height by all aerosol  
458 components. The restricted PBL development by BC absorption in our work is consistent with  
459 that identified previously (Ding et al., 2016; Petäjä et al., 2016). Using a radiative transfer  
460 model, Zhang et al. (2020) shows large strongly positive radiative forcing in the atmosphere  
461 and strongly negative radiative forcing at the surface by BC aging, consistent with those of the  
462 maximal estimates at about noontime from our calculations (Fig. 5i,f).

### 463 **3.5. Aerosol direct radiative forcing**

464 The aerosol direct radiative forcing during regional haze also exhibits a profound  
465 climatic effect (Ramanathan et al., 2007). Fig. 7 shows that the total aerosol radiative forcing  
466 at the surface (SFC) and in the atmosphere (ATM) during the haze episodes EP1 (EP2) are -  
467 87.8 (-62.8)  $W m^{-2}$  and 82.2 (56.9)  $W m^{-2}$ , respectively. The positive radiative forcing by all

Deleted: 4

469 aerosols in the atmosphere is dominated by that of aged BC, which accounts for 80% of the  
470 total radiative forcing for both episodes. The net radiative forcing at the top of the atmosphere  
471 (TOA) by all aerosols for EP1 (EP2) is around -5.6 (-5.9) W m<sup>-2</sup>, much smaller than the non-  
472 BC case with a large negative value of -36.8 (-26.0) W m<sup>-2</sup>. The strong cooling at the surface  
473 is largely canceled out by the strong warming in the atmosphere under the polluted condition,  
474 leading to a small net TOA forcing. Clearly, BC aging contributes significantly to cooling at  
475 the surface and warming aloft and, hence, the overall radiative budget during the polluted  
476 periods. Climatologically, the aerosol TOA forcing on the regional/national level has been  
477 shown to be nearly zero or slightly positive in China (Li et al., 2007; Ramanathan et al., 2007;  
478 Ding et al., 2016), also demonstrating that the large positive forcing by absorbing aerosols  
479 greatly compensates the negative forcing by the non-absorbing aerosols (Table S1). Therefore,  
480 regional global warming is likely mitigated by reducing BC emissions (Wang et al., 2015b).

#### 481 **4. Conclusions**

482 In this work, we analyzed the temporal and spatial characteristics of PM pollution  
483 during severe haze events over NCP, by examining ground-based measurements and satellite  
484 observations. Severe haze occurs frequently over this region, evident from a periodic (4-7 days)  
485 cycle of highly elevated PM pollution. The PM evolutions among the three megacities (Beijing,  
486 Baoding and Shijiazhuang) exhibit a remarkable similarity during the haze events, showing  
487 nearly synchronized temporal variations in the PM levels. The similar timing and magnitude  
488 in the peak PM<sub>2.5</sub> concentrations among the three megacities indicate significant *in-situ* PM  
489 production. Satellite measurements show that the AOD hotspots during the polluted period are  
490 co-located with the three megacities, but are distinct from seasonal and annual AOD means,  
491 indicating the importance of urban emissions (mainly traffic emissions consisting of  
492 anthropogenic VOCs and NO<sub>x</sub>). *In-situ* PM production occurs most efficiently over the

493 megacities, and urban sources relevant to traffic emissions play a critical role in regional severe  
494 haze formation.

495 Our result reveals that the rapid photochemistry drives the PM production during the  
496 transition period. There exist concurrent increases in OOA and PM<sub>2.5</sub> concentrations and a  
497 strong correlation between OOA and O<sub>x</sub> concentrations during this period. The [OOA]/[O<sub>x</sub>]  
498 ratio in Beijing is much higher than that in Mexico City and Houston, attributable to much  
499 higher level of gaseous precursors (i.e., anthropogenic VOCs and NO<sub>x</sub>) in Beijing than the  
500 other two cities. The correlation between [OOA] and [O<sub>x</sub>], however, vanishes during the  
501 polluted period, when O<sub>3</sub> production is significantly suppressed because of reduced solar  
502 ultraviolet radiation and inefficient photooxidation (Wu et al., 2020; Peng et al., 2021). The  
503 continuing increases in PM<sub>2.5</sub> and OOA with decreasing O<sub>x</sub> during the polluted period implies  
504 a key role of multiphase chemistry in driving the haze severity, when the RH level is  
505 significantly elevated. The continuous growth in PM<sub>2.5</sub> and OOA during the polluted period  
506 has been explained by an increasing importance of heterogeneous chemistry to contribute to  
507 sulfate, nitrate, and SOA formation (Wang et al., 2016a; An et al., 2019; Peng et al., 2021;  
508 Zhang et al., 2021).

509 Using the WRF model coupled with an explicit aerosol radiative module, we elucidated  
510 the underlying mechanism relevant to the haze-PBL interactions, showing a positive feedback  
511 to haze formation at the ground level. The PBL height is largely reduced under the polluted  
512 condition, since the PBL is markedly suppressed (as indicated by the reduced TKE and  
513 weakened updraft), because of strong aerosol heating in the atmosphere and strong cooling at  
514 the surface. The PM concentration near the surface accumulates significantly in a compressed  
515 PBL, since PM dispersion is unfavorable in the stratified and collapsed PBL, leading to  
516 continuous growth and accumulation of PM over multiple days. Calculations using the  
517 modified Nozaki's equation shows that the suppressed PBL results in a great enhancement of

518 atmospheric moisture near the surface. A more humid condition leads to hygroscopic growth  
519 of aerosol particles and more efficient multiphase PM production. Therefore, haze development  
520 near the surface is considerably exacerbated because of the positive feedback in responding to  
521 the atmospheric moisture and thermodynamic/dynamic conditions to amplify the haze severity.

522 Our combined observational analysis of the temporal/spatial PM distributions and  
523 modeling unravel a dominant regional characteristic for severe haze evolution in the NCP  
524 region, showing rapid *in-situ* PM production and inefficient transport, both of which are  
525 amplified by air stabilization. On the other hand, regional transport sufficiently disperses the  
526 gaseous aerosol precursors (SO<sub>2</sub>, NO<sub>x</sub>, VOCs, and NH<sub>3</sub>) during the clean period, which  
527 subsequently result in rapid *in-situ* PM production via photochemistry during the transition  
528 period and via multiphase chemistry during the polluted period.

529 The modeling simulations on two haze episodes indicate important regional climatic  
530 effects. The net TOA forcing for the two hazy days is about of -5.6 ~ -5.9 W m<sup>-2</sup>, showing  
531 strong negative radiative forcing (cooling) of -63 to -88 W m<sup>-2</sup> at the surface and strong positive  
532 radiative forcing (warming) of 57 to 82 W m<sup>-2</sup> in the atmosphere. BC represents the dominant  
533 contributor to the positive aerosol radiative forcing in the atmosphere, thus playing a significant  
534 role in the haze-PBL interaction. Specifically, BC aging contributes to more than 30% of the  
535 PBL collapse induced by total aerosols and about 50% of the TOA positive radiative forcing.  
536 Our work highlights the necessity to better understand the BC aging process and improve  
537 representation in atmospheric models for accurate assessment of the aerosol climatic effects.  
538 We conclude that reduction in BC emissions achieves co-benefits, which improve local and  
539 regional air quality by minimizing air stagnation and mitigate the global warming by alleviating  
540 the positive direct radiative forcing.

541 **Acknowledgement**

542           This work was partially supported by a collaborative Program between the Texas A&M  
543 University (TAMU) and the Natural Science Foundation of China (NSFC). R.Z. acknowledged  
544 additional support by the Robert A. Welch Foundation (Grant A-1417). The modeling portion  
545 of this research was conducted at the TAMU High Performance Research Computing. We  
546 thanked Hong-Bin Chen and Philippe Goloub for the data at the Beijing AERONET site.

547

548 **References**

- 549 [Aiken, A. C., Salcedo, D., Cubison, M. J., Huffman, J. A., DeCarlo, P. F., Ulbrich, I. M.,](#)  
550 [Docherty, K. S., Sueper, D., Kimmel, J. R., Worsnop, D. R., Trimborn, A., Northway, M.,](#)  
551 [Stone, E. A., Schauer, J. J., Volkamer, R. M., Fortner, E., de Foy, B., Wang, J., Laskin,](#)  
552 [A., Shutthanandan, V., Zheng, J., Zhang, R., Gaffney, J., Marley, N. A., Paredes-](#)  
553 [Miranda, G., Arnott, W. P., Molina, L. T., Sosa, G., and Jimenez, J. L.: Mexico City](#)  
554 [aerosol analysis during MILAGRO using high resolution aerosol mass spectrometry at](#)  
555 [the urban supersite \(T0\) – Part 1: Fine particle composition and organic source](#)  
556 [apportionment, Atmos. Chem. Phys., 9, 6633–6653, \[https://doi.org/10.5194/acp-9-6633-\]\(https://doi.org/10.5194/acp-9-6633-2009\)](#)  
557 [2009, 2009.](#)
- 558 An, Z. S., Huang, R. J., Zhang, R. Y., Tie, X. X., Li, G. H., Cao, J. J., Zhou, W. J., Shi, Z. G.,  
559 Han, Y. M., Gu, Z. L., and Ji, Y. M.: Severe haze in northern China: A synergy of  
560 anthropogenic emissions and atmospheric processes, Proc. Natl. Acad. Sci. USA, 116,  
561 8657-8666, 10.1073/pnas.1900125116, 2019.
- 562 Atkinson, R.: Atmospheric chemistry of VOCs and NOx, Atmos. Environ., 34, 2063-2101,  
563 [http://dx.doi.org/10.1016/S1352-2310\(99\)00460-4](http://dx.doi.org/10.1016/S1352-2310(99)00460-4), 2000.
- 564 Bond, T. C., Doherty, S. J., Fahey, D. W., Forster, P. M., Berntsen, T., DeAngelo, B. J.,  
565 Flanner, M. G., Ghan, S., Kärcher, B., Koch, D., Kinne, S., Kondo, Y., Quinn, P. K.,  
566 Sarofim, M. C., Schultz, M. G., Schulz, M., Venkataraman, C., Zhang, H., Zhang, S.,  
567 Bellouin, N., Guttikunda, S. K., Hopke, P. K., Jacobson, M. Z., Kaiser, J. W., Klimont,  
568 Z., Lohmann, U., Schwarz, J. P., Shindell, D., Storelvmo, T., Warren, S. G., and Zender,  
569 C. S.: Bounding the role of black carbon in the climate system: A scientific assessment, J.  
570 Geophys. Res.: Atmos., 118, 5380-5552, 10.1002/jgrd.50171, 2013.



571 Bouarar, I., Wang, X. M., and Brasseur, G. P.: Air Pollution in Eastern Asia: An Integrated  
572 Perspective Preface, *Issi Sci Rep Ser*, 16, V-Viii, Book\_Do [10.1007/978-3-319-59489-7](https://doi.org/10.1007/978-3-319-59489-7),  
573 2017.

574 Cai, W., Li, K., Liao, H., Wang, H., and Wu, L.: Weather conditions conducive to Beijing  
575 severe haze more frequent under climate change, *Nature Clim. Change*, 7, 257,  
576 [10.1038/nclimate3249](https://doi.org/10.1038/nclimate3249), 2017.

577 Che, H., Xia, X., Zhu, J., Li, Z., Dubovik, O., Holben, B., Goloub, P., Chen, H., Estelles, V.,  
578 Cuevas-Agullo, E., Blarel, L., Wang, H., Zhao, H., Zhang, X., Wang, Y., Sun, J., Tao, R.,  
579 Zhang, X., and Shi, G.: Column aerosol optical properties and aerosol radiative forcing  
580 during a serious haze-fog month over North China Plain in 2013 based on ground-based  
581 sunphotometer measurements, *Atmos. Chem. Phys.*, 14, 2125-2138, [10.5194/acp-14-](https://doi.org/10.5194/acp-14-2125-2014)  
582 [2125-2014](https://doi.org/10.5194/acp-14-2125-2014), 2014.

583 Ding, A. J., Huang, X., Nie, W., Sun, J. N., Kerminen, V. M., Petäjä, T., Su, H., Cheng, Y.  
584 F., Yang, X. Q., Wang, M. H., Chi, X. G., Wang, J. P., Virkkula, A., Guo, W. D., Yuan,  
585 J., Wang, S. Y., Zhang, R. J., Wu, Y. F., Song, Y., Zhu, T., Zilitinkevich, S., Kulmala,  
586 M., and Fu, C. B.: Enhanced haze pollution by black carbon in megacities in China,  
587 *Geophys. Res. Lett.*, 43, 2873–2879, [10.1002/2016GL067745](https://doi.org/10.1002/2016GL067745), 2016.

588 Fan, J., and Zhang, R. Atmospheric oxidation mechanism of isoprene. *Environ. Chem.*, 1,  
589 140-149, 2004.

590 Fan, J., Zhang, R., Tao, W.-K., and Mohr, K. I.: Effects of aerosol optical properties on deep  
591 convective clouds and radiative forcing, *J. Geophys. Res.*, 113, D08209,  
592 [10.1029/2007jd009257](https://doi.org/10.1029/2007jd009257), 2008.

593 Guo, S., Hu, M., Zamora, M. L., Peng, J., Shang, D., Zheng, J., Du, Z., Wu, Z., Shao, M.,  
594 Zeng, L., Molina, M. J., and Zhang, R.: Elucidating severe urban haze formation in  
595 China, *Proc. Natl. Acad. Sci. U S A*, 111, 17373-17378, [10.1073/pnas.1419604111](https://doi.org/10.1073/pnas.1419604111), 2014.

596 Guo, S., Hu, M., Peng, J. F., Wu, Z. J., Zamora, M. L., Shang, D. J., Du, Z. F., Zheng, J.,  
597 Fang, X., Tang, R. Z., Wu, Y. S., Zeng, L. M., Shuai, S. J., Zhang, W. B., Wang, Y., Ji,  
598 Y. M., Li, Y. X., Zhang, A. L., Wang, W. G., Zhang, F., Zhao, J. Y., Gong, X. L., Wang,  
599 C. Y., Molina, M. J., and Zhang, R. Y.: Remarkable nucleation and growth of ultrafine  
600 particles from vehicular exhaust, *Proc. Natl. Acad. Sci. USA*, 117, 3427-3432,  
601 10.1073/pnas.1916366117, 2020.

602 Guo, S., Hu, M., Lin, Y., Gomez-Hernandez, M., Zamora, M. L., Peng, J. F., Collins, D. R.,  
603 and Zhang, R. Y.: OH-Initiated Oxidation of m-Xylene on Black Carbon Aging, *Environ.*  
604 *Sci. Technol.*, 50, 8605-8612, 10.1021/acs.est.6b01272, 2016.

605 Gustafsson, Ö., and Ramanathan, V.: Convergence on climate warming by black carbon  
606 aerosols, *Proc. Natl. Acad. Sci. USA*, 113, 4243-4245, 10.1073/pnas.1603570113, 2016.

607 He, C., Liou, K. N., Takano, Y., Zhang, R., Levy Zamora, M., Yang, P., Li, Q., and Leung, L.  
608 R.: Variation of the radiative properties during black carbon aging: theoretical and  
609 experimental intercomparison, *Atmos. Chem. Phys.*, 15, 11967-11980, 10.5194/acp-15-  
610 11967-2015, 2015.

611 Intergovernmental Panel on Climate Change (IPCC). *Climate Change 2013: The Physical*  
612 *Science Basis. Contribution of Working Group I to the Fifth Assessment Report of the*  
613 *Intergovernmental Panel on Climate Change*. Cambridge University Press, **2013**.

614 Khalizov, A. F., Lin, Y., Qiu, C., Guo, S., Collins, D., and Zhang, R.: Role of OH-initiated  
615 oxidation of isoprene in aging of combustion soot, *Environ. Sci. Technol.*, 47, 2254-2263,  
616 10.1021/es3045339, 2013.

617 Johnson, N. M., Hoffmann, A. R., Behlen, J. C., Lau, C., Pendleton, D., Harvey, N., Shore,  
618 R., Li, Y. X., Chen, J. S., Tian, Y. A., and Zhang, R. Y.: Air pollution and children's  
619 health-a review of adverse effects associated with prenatal exposure from fine to ultrafine

620 particulate matter, *Environ. Health. Prev.*, 26, ARTN 72, 10.1186/s12199-021-00995-5,  
621 2021.

622 Levy, R. C., Leptoukh, G. G., Kahn, R., Zubko, V., Gopalan, A., and Remer, L. A.: A  
623 Critical Look at Deriving Monthly Aerosol Optical Depth From Satellite Data, *Ieee T*  
624 *Geosci Remote*, 47, 2942-2956, Doi 10.1109/Tgrs.2009.2013842, 2009.

625 Li, G., Wang, Y., and Zhang, R.: Implementation of a two-moment bulk microphysics  
626 scheme to the WRF model to investigate aerosol-cloud interaction, *J. Geophys. Res.*, 113,  
627 D15211, 10.1029/2007jd009361, 2008.

628 Li, P., Yan, R., Yu, S., Wang, S., Liu, W., and Bao, H.: Reinstatement regional transport of PM<sub>2.5</sub>  
629 as a major cause of severe haze in Beijing, *Proc. Natl. Acad. Sci. USA*, 112, E2739-  
630 E2740, 10.1073/pnas.1502596112, 2015.

631 Li, Y., Zhao, J., Wang, Y., Seinfeld, J. H., and Zhang, R.: Multigeneration Production of  
632 Secondary Organic Aerosol from Toluene Photooxidation, *Environmental science &*  
633 *technology*, 55, 8592-8603, 10.1021/acs.est.1c02026, 2021a.

634 Li, Y., Ji, Y., Zhao, J., Wang, Y., Shi, Q., Peng, J., Wang, Y., Wang, C., Zhang, F., Wang,  
635 Y., Seinfeld, J. H., and Zhang, R.: Unexpected Oligomerization of Small  $\alpha$ -Dicarbonyls  
636 for Secondary Organic Aerosol and Brown Carbon Formation, *Environmental science &*  
637 *technology*, 55, 4430-4439, 10.1021/acs.est.0c08066, 2021b.

638 Li, Z., Xia, X., Cribb, M., Mi, W., Holben, B., Wang, P., Chen, H., Tsay, S.-C., Eck, T. F.,  
639 Zhao, F., Dutton, E. G., and Dickerson, R. E.: Aerosol optical properties and their  
640 radiative effects in northern China, *J. Geophys. Res.: Atmos.*, 112, D22S01,  
641 10.1029/2006JD007382, 2007.

642 Li, Z., Guo, J., Ding, A., Liao, H., Liu, J., Sun, Y., Wang, T., Xue, H., Zhang, H., and Zhu,  
643 B.: Aerosol and Boundary-Layer Interactions and Impact on Air Quality, *Natl. Sci. Rev.*,  
644 nwx117-nwx117, 10.1093/nsr/nwx117, 2017.

645 Li, Z. Q., Wang, Y., Guo, J. P., Zhao, C. F., Cribb, M., Dong, X. Q., Fan, J. W., Gong, D. Y.,  
646 Huang, J. P., Jiang, M. J., Jiang, Y. Q., Lee, S. S., Li, H., Li, J. M., Liu, J. J., Qian, Y.,  
647 Rosenfeld, D., Shan, S. Y., Sun, Y. L., Wang, H. J., Xin, J. Y., Yan, X., Yang, X., Yang,  
648 X. Q., Zhang, F., and Zheng, Y. T.: East Asian Study of Tropospheric Aerosols and their  
649 Impact on Regional Clouds, Precipitation, and Climate (EAST-AIR(CPC)), *J. Geophys.*  
650 *Res.-Atmos.*, 124, 13026-13054, 10.1029/2019jd030758, 2019.

651 Lin, Y., Wang, Y., Pan, B., Hu, J., Liu, Y., and Zhang, R.: Distinct Impacts of Aerosols on an  
652 Evolving Continental Cloud Complex during the RACORO Field Campaign, *J. Atmos.*  
653 *Sci.*, 73, 3681-3700, doi:10.1175/JAS-D-15-0361.1, 2016.

654 Liu, J., F. Zhang, W. Xu, Y. Sun, L. Chen, S. Li, J. Ren, B. Hu, H. Wu, and R. Zhang,  
655 Hygroscopicity of organic aerosols linked to formation mechanisms. *Geophys. Res. Lett.*  
656 48, doi.org/10.1029/2020GL091683, 2021.

657 Liu, X. G., Li, J., Qu, Y., Han, T., Hou, L., Gu, J., Chen, C., Yang, Y., Liu, X., Yang, T.,  
658 Zhang, Y., Tian, H., and Hu, M.: Formation and evolution mechanism of regional haze: a  
659 case study in the megacity Beijing, China, *Atmos. Chem. Phys.*, 13, 4501-4514, DOI  
660 10.5194/acp-13-4501-2013, 2013.

661 Mallet, M., Roger, J. C., Despiiau, S., Putaud, J. P., and Dubovik, O.: A study of the mixing  
662 state of black carbon in urban zone, *J. Geophys. Res.: Atmos.*, 109, n/a-n/a,  
663 10.1029/2003JD003940, 2004.

664 Meier, J., Wehner, B., Massling, A., Birmili, W., Nowak, A., Gnauk, T., Brüggemann, E.,  
665 Herrmann, H., Min, H., and Wiedensohler, A.: Hygroscopic growth of urban aerosol  
666 particles in Beijing (China) during wintertime: a comparison of three experimental  
667 methods, *Atmos. Chem. Phys.*, 9, 6865-6880, 10.5194/acp-9-6865-2009, 2009.

668 Menon, S., Hansen, J., Nazarenko, L., and Luo, Y.: Climate Effects of Black Carbon  
669 Aerosols in China and India, *Science*, 297, 2250-2253, 10.1126/science.1075159, 2002.

670 Molina, L. T.: Introductory lecture: air quality in megacities, *Faraday Discuss*, 226, 9-52,  
671 10.1039/d0fd00123f, 2021.

672 Nozaki, K. Y.: *Mixing Depth Model Using Hourly Surface Observations Report 7053*, USAF  
673 Environmental Technical Applications Center, 1973.

674 Pasquill, F.: The Estimation of the Dispersion of Windborne Material, *Meteorological*  
675 *Magazin*, 90, 33-49, 1961.

676 Peng, J., Hu, M., Guo, S., Du, Z., Zheng, J., Shang, D., Levy Zamora, M., Zeng, L., Shao,  
677 M., Wu, Y.-S., Zheng, J., Wang, Y., Glen, C. R., Collins, D. R., Molina, M. J., and  
678 Zhang, R.: Markedly enhanced absorption and direct radiative forcing of black carbon  
679 under polluted urban environments, *Proc. Natl. Acad. Sci. USA*, 4266–4271,  
680 10.1073/pnas.1602310113, 2016.

681 Peng, J., Hu, M., Guo, S., Du, Z., Shang, D., Zheng, J., Zheng, J., Zeng, L., Shao, M., Wu,  
682 Y., Collins, D., and Zhang, R.: Ageing and hygroscopicity variation of black carbon  
683 particles in Beijing measured by a quasi-atmospheric aerosol evolution study  
684 (QUALITY) chamber, *Atmos. Chem. Phys.*, 17, 10333-10348, 10.5194/acp-17-10333-  
685 2017, 2017.

686 Peng, J. F., Hu, M., Shang, D. J., Wu, Z. J., Du, Z. F., Tan, T. Y., Wang, Y. N., Zhang, F.,  
687 and Zhang, R. Y.: Explosive Secondary Aerosol Formation during Severe Haze in the  
688 North China Plain, *Environ. Sci. Technol.*, 55, 2189-2207, 10.1021/acs.est.0c07204,  
689 2021.

690 Petäjä, T., Järvi, L., Kerminen, V. M., Ding, A. J., Sun, J. N., Nie, W., Kujansuu, J.,  
691 Virkkula, A., Yang, X., Fu, C. B., Zilitinkevich, S., and Kulmala, M.: Enhanced air  
692 pollution via aerosol-boundary layer feedback in China, *Sci. Rep.*, 6, 18998,  
693 10.1038/srep18998, 2016.

694 Qian, Y., Leung, R.L., Ghan, S. J., and Giorgi, F.: Regional climate effects of aerosols over  
695 China: modeling and observation, *Tellus B*, 55, 914-934, 10.1046/j.1435-  
696 6935.2003.00070.x, 2003.

697 Qian, Y, Gong, D., Fan, J., Leung, R.L., Bennartz, R., Chen, D., Wang, W.: Heavy pollution  
698 suppresses light rain in China: Observations and modeling, *J. Geophys. Res.: Atmos.*,  
699 114, 10.1029/2008JD011575, 2009.

700 Ramanathan, V., Li, F., Ramana, M. V., Praveen, P. S., Kim, D., Corrigan, C. E., Nguyen, H.,  
701 Stone, E. A., Schauer, J. J., Carmichael, G. R., Adhikary, B., and Yoon, S. C.:  
702 Atmospheric brown clouds: Hemispherical and regional variations in long-range  
703 transport, absorption, and radiative forcing, *J. Geophys. Res.: Atmos.*, 112, D22S21,  
704 10.1029/2006JD008124, 2007.

705 Rychlik, K. A., Secret, J. R., Lau, C., Pulczynski, J., Zamora, M. L., Leal, J., Langley, R.,  
706 Myatt, L. G., Raju, M., Chang, R. C. A., Li, Y. X., Golding, M. C., Rodrigues-Hoffmann,  
707 A., Molina, M. J., Zhang, R. Y., and Johnson, N. M.: In utero ultrafine particulate matter  
708 exposure causes offspring pulmonary immunosuppression, *Proc. Natl. Acad. Sci. USA*,  
709 116, 3443-3448, 10.1073/pnas.1816103116, 2019.

710 Suh, I., Lei, W., and Zhang, R. Experimental and theoretical studies of isoprene reaction with  
711 NO<sub>3</sub>. *J. Phys. Chem.* 105, 6471-6478, 2001.

712 Sun, Y. L., Jiang, Q., Wang, Z. F., Fu, P. Q., Li, J., Yang, T., and Yin, Y.: Investigation of  
713 the Sources and Evolution Processes of Severe Haze Pollution in Beijing in January 2013,  
714 *J. Geophys Res.-Atmos.*, 119, 4380-4398, Doi 10.1002/2014jd021641, 2014.

715 Tang, G., Zhang, J., Zhu, X., Song, T., Munkel, C., Hu, B., Schäfer, K., Liu, Z., Zhang, J.,  
716 Wang, L., Xin, J., Suppan, P., and Wang, Y.: Mixing layer height and its implications for  
717 air pollution over Beijing, China, *Atmos. Chem. Phys.*, 16, 2459-2475, 10.5194/acp-16-  
718 2459-2016, 2016a.

719 Tang, W., Qin, J., Yang, K., Liu, S., Lu, N., and Niu, X.: Retrieving high-resolution surface  
720 solar radiation with cloud parameters derived by combining MODIS and MTSAT data,  
721 *Atmos. Chem. Phys.*, 16, 2543-2557, 10.5194/acp-16-2543-2016, 2016b.

722 Tie, X., Huang, R.-J., Cao, J., Zhang, Q., Cheng, Y., Su, H., Chang, D., Pöschl, U.,  
723 Hoffmann, T., Dusek, U., Li, G., Worsnop, D. R., and O'Dowd, C. D.: Severe Pollution  
724 in China Amplified by Atmospheric Moisture, *Sci. Rep.*, 7, 15760, 10.1038/s41598-017-  
725 15909-1, 2017.

726 Wallace, J. M., and Hobbs, P. V.: *Atmospheric Science*, Second Edition, Elsevier, 2005.

727 Wang, G., Zhang, R., Gomez, M. E., Yang, L., Levy Zamora, M., Hu, M., Lin, Y., Peng, J.,  
728 Guo, S., Meng, J., Li, J., Cheng, C., Hu, T., Ren, Y., Wang, Y., Gao, J., Cao, J., An, Z.,  
729 Zhou, W., Li, G., Wang, J., Tian, P., Marrero-Ortiz, W., Secret, J., Du, Z., Zheng, J.,  
730 Shang, D., Zeng, L., Shao, M., Wang, W., Huang, Y., Wang, Y., Zhu, Y., Li, Y., Hu, J.,  
731 Pan, B., Cai, L., Cheng, Y., Ji, Y., Zhang, F., Rosenfeld, D., Liss, P. S., Duce, R. A.,  
732 Kolb, C. E., and Molina, M. J.: Persistent sulfate formation from London Fog to Chinese  
733 haze, *Proc. Natl. Acad. Sci. USA*, 113, 13630-13635, 10.1073/pnas.1616540113, 2016a.

734 Wang, H., Shi, G. Y., Zhang, X. Y., Gong, S. L., Tan, S. C., Chen, B., Che, H. Z., and Li, T.:  
735 Mesoscale modelling study of the interactions between aerosols and PBL meteorology  
736 during a haze episode in China Jing-Jin-Ji and its near surrounding region – Part 2:  
737 Aerosols' radiative feedback effects, *Atmos. Chem. Phys.*, 15, 3277-3287, 10.5194/acp-  
738 15-3277-2015, 2015a.

739 Wang, J., Allen, D. J., Pickering, K. E., Li, Z., and He, H.: Impact of aerosol direct effect on  
740 East Asian air quality during the EAST-AIRE campaign, *J. Geophys. Res.: Atmos.*, 121,  
741 6534-6554, 10.1002/2016JD025108, 2016b.

742 Wang, Y., Wan, Q., Meng, W., Liao, F., Tan, H., and Zhang, R.: Long-term impacts of  
743 aerosols on precipitation and lightning over the Pearl River Delta megacity area in China,  
744 *Atmos. Chem. Phys.*, 11, 12421-12436, 10.5194/acp-11-12421-2011, 2011.

745 Wang, Y., Che, H., Ma, J., Wang, Q., Shi, G., Chen, H., Goloub, P., and Hao, X.: Aerosol  
746 radiative forcing under clear, hazy, foggy, and dusty weather conditions over Beijing,  
747 China, *Geophys. Res. Lett.*, 36, n/a-n/a, 10.1029/2009GL037181, 2009.

748 Wang, Y., Khalizov, A., Levy, M., and Zhang, R. Y.: New Directions: Light absorbing  
749 aerosols and their atmospheric impacts, *Atmos. Environ.*, 81, 713-715,  
750 10.1016/j.atmosenv.2013.09.034, 2013.

751 Wang, Y., Zhang, R., and Saravanan, R.: Asian pollution climatically modulates mid-latitude  
752 cyclones following hierarchical modelling and observational analysis, *Nat. commun.*, 5,  
753 3098, 10.1038/ncomms4098, 2014a.

754 Wang, Y., Wang, M., Zhang, R., Ghan, S. J., Lin, Y., Hu, J., Pan, B., Levy, M., Jiang, J. H.,  
755 and Molina, M. J.: Assessing the effects of anthropogenic aerosols on Pacific storm track  
756 using a multiscale global climate model, *Proc. Natl. Acad. Sci. U S A*, 111, 6894-6899,  
757 10.1073/pnas.1403364111, 2014b.

758 Wang, Y., Lee, K.-H., Lin, Y., Levy, M., and Zhang, R.: Distinct effects of anthropogenic  
759 aerosols on tropical cyclones, *Nature Clim. Change*, 4, 368-373, 10.1038/nclimate2144,  
760 2014c.

761 Wang, Y. S., Yao, L., Wang, L. L., Liu, Z. R., Ji, D. S., Tang, G. Q., Zhang, J. K., Sun, Y.,  
762 Hu, B., and Xin, J. Y.: Mechanism for the Formation of the January 2013 Heavy Haze  
763 Pollution Episode over Central and Eastern China, *Sci. China Earth Sci.*, 57, 14-25, DOI  
764 10.1007/s11430-013-4773-4, 2014d.



765 Wang, Z., Huang, X., and Ding, A.: Dome effect of black carbon and its key influencing  
766 factors: A one-dimensional modelling study, *Atmos. Chem. Phys. Discuss.*, 2017, 1-29,  
767 10.5194/acp-2017-967, 2017.

768 Wang, Z. L., Zhang, H., and Zhang, X. Y.: Simultaneous reductions in emissions of black  
769 carbon and co-emitted species will weaken the aerosol net cooling effect, *Atmos. Chem.*  
770 *Phys.*, 15, 3671-3685, 10.5194/acp-15-3671-2015, 2015b.

771 Wilcox, E. M., Thomas, R. M., Praveen, P. S., Pistone, K., Bender, F. A.-M., and  
772 Ramanathan, V.: Black carbon solar absorption suppresses turbulence in the atmospheric  
773 boundary layer, *Proc. Natl. Acad. Sci. USA*, 113, 11794-11799,  
774 10.1073/pnas.1525746113, 2016.

775 Wood, E. C., Canagaratna, M. R., Herndon, S. C., Onasch, T. B., Kolb, C. E., Worsnop, D.  
776 R., Kroll, J. H., Knighton, W. B., Seila, R., Zavala, M., Molina, L. T., DeCarlo, P. F.,  
777 Jimenez, J. L., Weinheimer, A. J., Knapp, D. J., Jobson, B. T., Stutz, J., Kuster, W. C.,  
778 and Williams, E. J.: Investigation of the correlation between odd oxygen and secondary  
779 organic aerosol in Mexico City and Houston, *Atmos. Chem. Phys.*, 10, 8947-8968,  
780 10.5194/acp-10-8947-2010, 2010.

781 Wu, G., Li, Z., Fu, C., Zhang, X., Zhang, R., Zhang, R., Zhou, T., Li, J., Li, J., Zhou, D., Wu,  
782 L., Zhou, L., He, B. and Huang, R. Advances in studying interactions between aerosols  
783 and monsoon in China, *Sci. China: Earth Sci.*, 59, 1–16, 10.1007/s11430-015-5198-z,  
784 2016.

785 Wu, G. Y., Brown, J., Zamora, M. L., Miller, A., Satterfield, M. C., Meininger, C. J.,  
786 Steinhauser, C. B., Johnson, G. A., Burghardt, R. C., Bazer, F. W., Li, Y. X., Johnson, N.  
787 M., Molina, M. J., and Zhang, R. Y.: Adverse organogenesis and predisposed long-term  
788 metabolic syndrome from prenatal exposure to fine particulate matter, *Proc. Natl. Acad.*  
789 *Sci. USA*, 116, 11590-11595, 10.1073/pnas.1902925116, 2019.

790 Wu, J. R., Bei, N. F., Hu, B., Liu, S. X., Wang, Y., Shen, Z. X., Li, X., Liu, L., Wang, R. N.,  
791 Liu, Z. R., Cao, J. J., Tie, X. X., Molina, L. T., and Li, G. H.: Aerosol-photolysis  
792 interaction reduces particulate matter during wintertime haze events, *Proc. Natl. Acad.*  
793 *Sci. USA*, 117, 9755-9761, 10.1073/pnas.1916775117, 2020.

794 Xia, X., Chen, H., Goloub, P., Zhang, W., Chatenet, B., and Wang, P.: A compilation of  
795 aerosol optical properties and calculation of direct radiative forcing over an urban region  
796 in northern China, *J. Geophys. Res.: Atmos.*, 112, 10.1029/2006JD008119, 2007.

797 Yuan, T., Li, Z., Zhang, R., and Fan, J. Increase of cloud droplet size with aerosol optical  
798 depth: An observation and modeling study, *J. Geophys. Res.*, 113, D04201,  
799 doi:10.1029/2007JD008632, 2008.

800 Zhang, F., Wang, Y., Peng, J. F., Chen, L., Sun, Y. L., Duan, L., Ge, X. L., Li, Y. X., Zhao, J.  
801 Y., Liu, C., Zhang, X. C., Zhang, G., Pan, Y. P., Wang, Y. S., Zhang, A. L., Ji, Y. M.,  
802 Wang, G. H., Hu, M., Molina, M. J., and Zhang, R. Y.: An unexpected catalyst dominates  
803 formation and radiative forcing of regional haze, *Proc. Natl. Acad. Sci. USA*, 117, 3960-  
804 3966, doi/10.1073/pnas.1919343117, 2020.

805 Zhang, R., Li, G. H., Fan, J. W., Wu, D. L., and Molina, M. J.: Intensification of Pacific  
806 storm track linked to Asian pollution, *Proc. Natl. Acad. Sci. USA*, 104, 5295-5299,  
807 10.1073/pnas.0700618104, 2007.

808 Zhang, R., Khalizov, A. F., Pagels, J., Zhang, D., Xue, H., and McMurry, P. H.: Variability in  
809 morphology, hygroscopicity, and optical properties of soot aerosols during atmospheric  
810 processing, *Proc. Natl. Acad. Sci. USA*, 105, 10291-10296, 10.1073/pnas.0804860105,  
811 2008.

812 Zhang, R., Wang, G., Guo, S., Zamora, M. L., Ying, Q., Lin, Y., Wang, W., Hu, M., and  
813 Wang, Y.: Formation of Urban Fine Particulate Matter, *Chem. Rev.*, 115, 3803-3855,  
814 10.1021/acs.chemrev.5b00067, 2015a.

815 Zhang, R., Guo, S., Levy Zamora, M., and Hu, M.: Reply to Li et al.: Insufficient evidence  
816 for the contribution of regional transport to severe haze formation in Beijing, Proc. Natl.  
817 Acad. Sci. USA, 112, E2741, 10.1073/pnas.1503855112, 2015b.

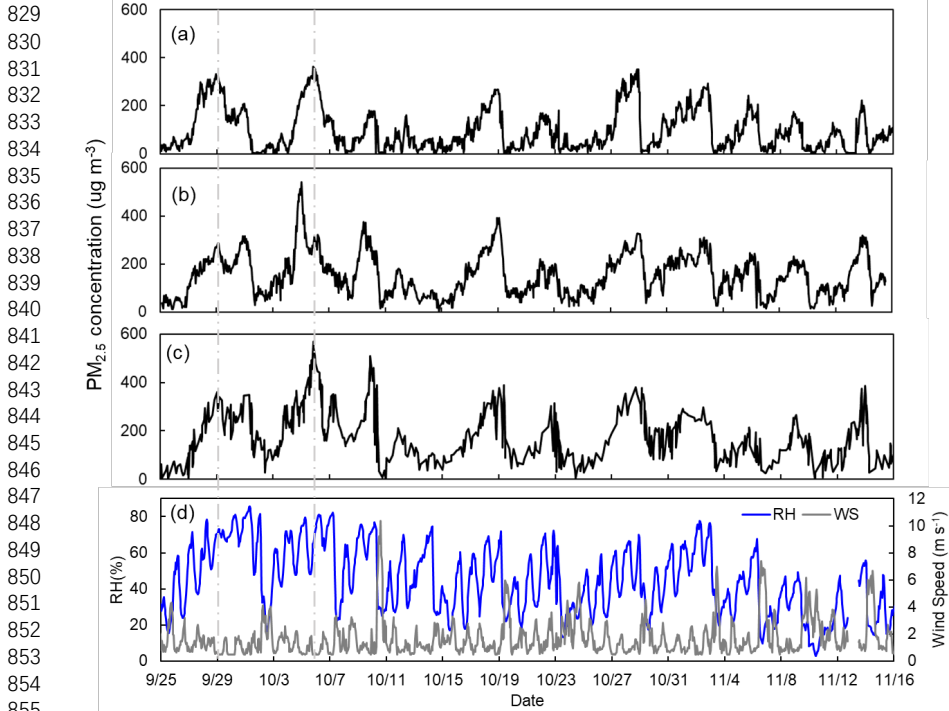
818 Zhang, R., N.M. Johnson, Y. Li: Establishing the exposure-outcome relation between  
819 airborne particulate matter and children's health, Thorax, 76, doi.org/10.1136/thoraxjnl-  
820 2021- 217017, 2021.

821 Zhang, X., Zhang, Q., Hong, C., Zheng, Y., Geng, G., Tong, D., Zhang, Y., and Zhang, X.:  
822 Enhancement of PM<sub>2.5</sub> concentrations by aerosol-meteorology interactions over China, J.  
823 Geophys. Res.: Atmos., 1179-1194, 10.1002/2017JD027524, 2018.

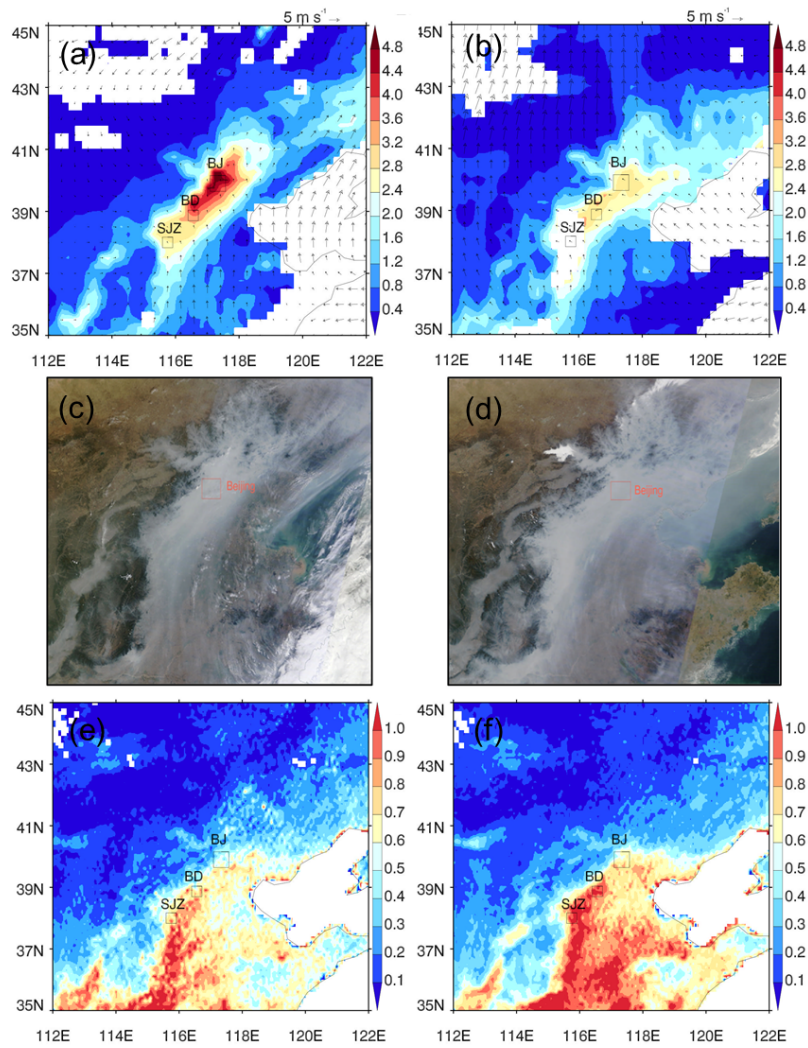
824 Zhao, J., Zhang, R., Fortner, E.C., and North, S.W.: Quantification of hydroxycarbonyls from  
825 OH-isoprene reactions, J. Am. Chem. Soc., 126, 2686-2687, 2004.

826 Zhao, J., Zhang, R., Misawa, K. and Shibuya, K. Experimental product study of the OH-  
827 initiated oxidation of m-xylene. J. Photoch. Photobio. A, 176, 199-207, 2005.

828

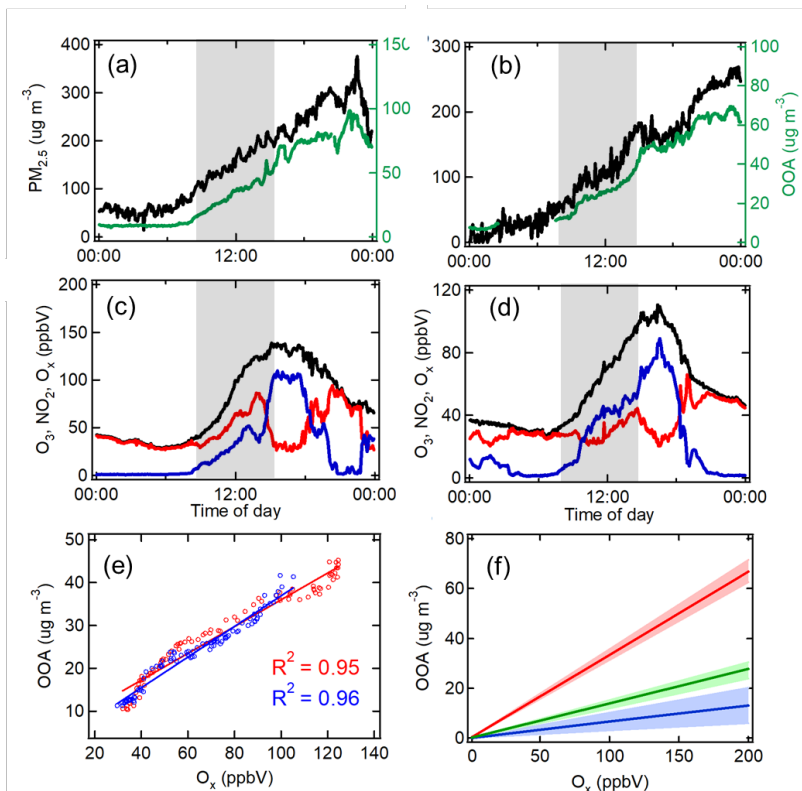


829  
830  
831  
832  
833  
834  
835  
836  
837  
838  
839  
840  
841  
842  
843  
844  
845  
846  
847  
848  
849  
850  
851  
852  
853  
854  
855  
856 **Figure 1.** Time series of PM<sub>2.5</sub> mass concentration measured at three megacities over North  
857 China Plain (NCP), including (a) Beijing, (b) Baoding, and (c) Shijiazhuang from 25  
858 September to 16 November, 2013, and (d) the associated relative humidity (RH, blue line) and  
859 10-m wind speed (grey line) in Beijing. The PM<sub>2.5</sub> mass concentration and meteorological  
860 fields in Beijing are taken from Guo et al. (2014), and the PM<sub>2.5</sub> data for Baoding and  
861 Shijiazhuang are taken from <https://air.cnemc.cn:18007/>. Two severe haze episodes from 25-  
862 29 September and from 2-7 October are selected as the case studies in this work, and the two  
863 vertical dash lines label the time for the peak PM<sub>2.5</sub> concentration in Beijing.  
864



865  
866

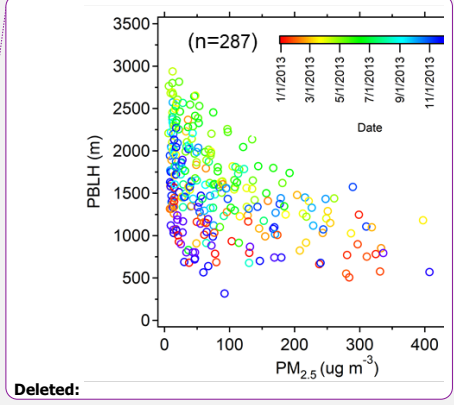
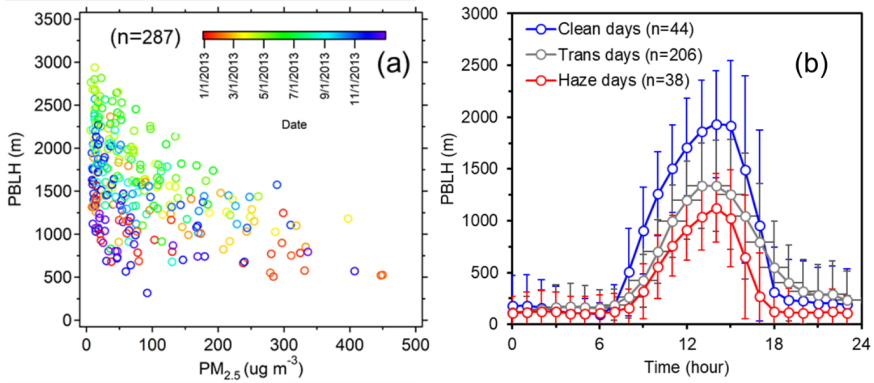
867 **Figure 2.** MODIS AOD (a-b) and visible images (c-d) illustrating the two severe haze episodes  
868 in Fig. 1. (a) and (c) correspond to 28 September, 2013, and (b) and (d) correspond to 5 October,  
869 2013. (e) and (f) represent MODIS AOD of fall seasonal and annual mean in 2013. The  
870 megacities of Beijing (BJ), Baoding (BD) and Shijiazhuang (SJZ) are marked as squares. Wind  
871 field imposed on (a) and (b) is based on ECMWF reanalysis data.



872  
 873 **Figure 3.** Temporal evolutions of measured PM<sub>2.5</sub> (black) and OOA (green) mass  
 874 concentrations (a-b) and O<sub>3</sub> (blue), NO<sub>2</sub> (red), and O<sub>x</sub> (black) mixing ratios (c-d) during the  
 875 early stages of the two haze episodes. (a) and (c) are for the episode starting on 27 September,  
 876 2013, and (b) and (d) are for the episode starting on 4 October, 2013. (e) represents linear  
 877 regression between O<sub>x</sub> and OOA on 27 September (red circles) and 4 October (blue circles),  
 878 2013. The grey shadings (a-d) represent the largest variation in O<sub>x</sub>, which covers both the clean  
 879 and transition periods. (f) corresponds to the ratios of [OOA] changes to [O<sub>x</sub>] changes  
 880 ( $\Delta[\text{OOA}]/\Delta[\text{O}_x]$ ) for Beijing (red), Mexico City (green) and Houston (blue). The ratios for  
 881 Beijing are derived from this study, and the ratios for Mexico City and Houston taken from  
 882 Wood et al. (2010). Color shadings in (f) represent the range between the minimum and  
 883 maximum ratios.

**Deleted:** ,

**Deleted:** using measurements at the transition periods (grey shadings (a-d)).

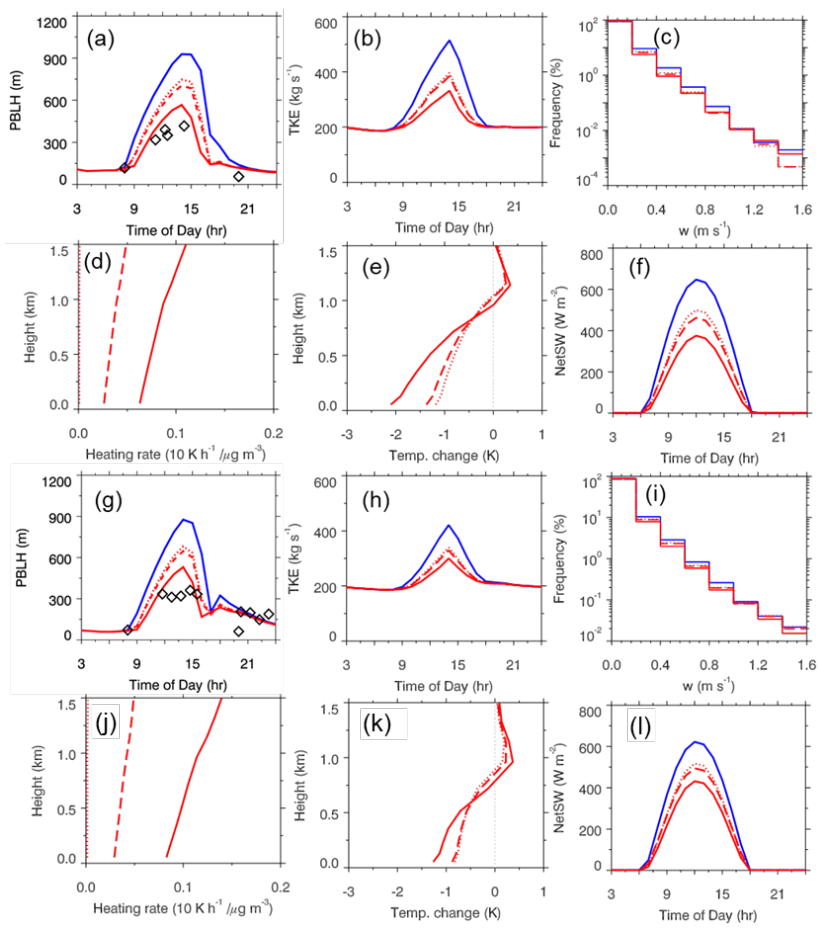


887

888 **Figure 4.** (a) Scattering plot for daily mean PBL height versus PM<sub>2.5</sub> concentration and (b)  
 889 mean diurnal variations of PBL height averaged over clean days (daily mean PM<sub>2.5</sub> < 30 μg  
 890 m<sup>-3</sup>), extremely hazy days (daily mean PM<sub>2.5</sub> > 200 μg m<sup>-3</sup>), and transition days (30 μg m<sup>-3</sup> <  
 891 daily mean PM<sub>2.5</sub> < 200 μg m<sup>-3</sup>) in 2013 at Beijing, China. *n* denotes the number of days used  
 892 for plotting. The vertical lines in (b) denote ±1 standard deviation. All the precipitation days  
 893 were filtered out.  
 894

Deleted:

Deleted: and

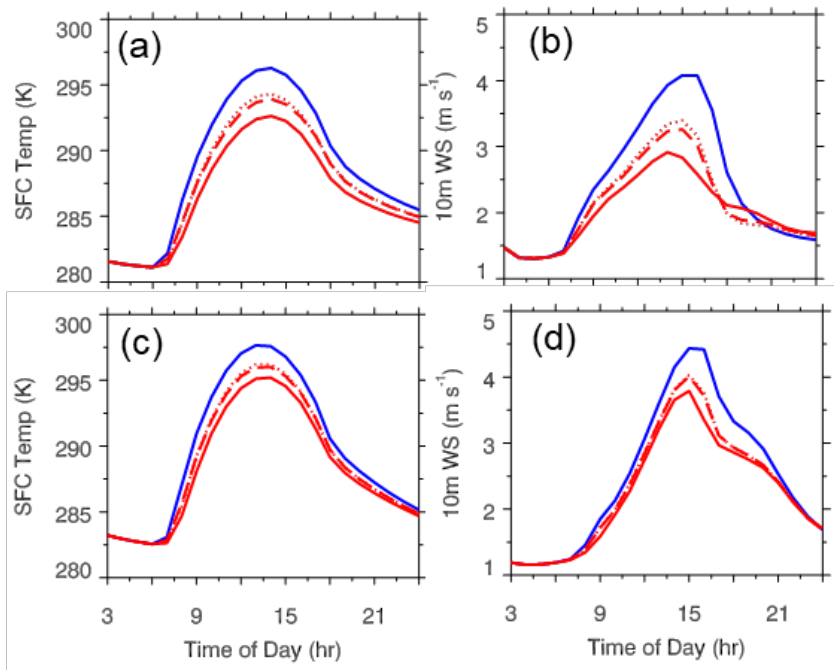


897

898 **Figure 5.** Simulated meteorological conditions and thermodynamic and dynamic feedbacks  
 899 under the clean conditions (blue solid) and the polluted conditions for the non-BC (red dot),  
 900 fresh-BC (red dashed), and aged-BC (red solid) cases. (a) and (g) correspond to simulated  
 901 diurnal variations of PBL height, (b) and (h) correspond to the diurnal variations of vertically  
 902 integrated TKE, (c) and (i) represent the frequency distribution of updraft. (d) and (j) are the  
 903 vertical profile of the shortwave heating rate per unit aerosol mass for the non-BC (red dot  
 904 line), fresh-BC (red dash line), and aged-BC (red solid line) cases. (e) and (k) are similar as  
 905 (d) and (j) but for the temperature changes. (f) and (l) are diurnal evolutions of net surface  
 906 shortwave radiation (NetSW). (a-f) are for EP1 and (g-l) are for EP2. The black hollow  
 907 squares in (a) and (g) denote measurements of PBL height from ceilometer.  
 908

Deleted:

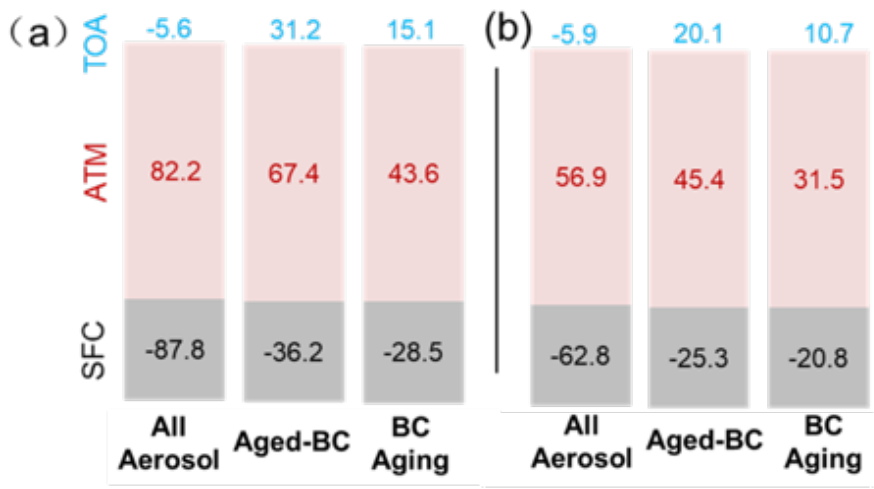




910

911 **Figure 6.** Temporal evolutions of surface temperatures (a and c) and 10-meter wind speeds (b  
 912 and d) under the clean conditions (blue solid) and the polluted conditions for the non-BC (red  
 913 dot), fresh-BC (red dashed), and aged-BC (red solid) cases. (a) and (b) correspond to EP1,  
 914 and (c) and (d) correspond to EP2.

915



916

917 **Figure 7.** Aerosol direct radiative forcing for total aerosol (left column), aged-BC (middle  
 918 column), and BC aging (right column) on the top of the atmosphere (TOA), in the atmosphere  
 919 (ATM), and at the surface (SFC) for two severe haze days in Beijing. (a) and (b) correspond to  
 920 EP1 and EP2, respectively. The forcing caused by BC aging corresponds to the difference in  
 921 the simulations between the fresh-BC and aged-BC cases. The number denotes radiative  
 922 forcing in the unit of  $W m^{-2}$ .  
 923

924  
925

**Table 1.** List of numerical experiments.

<u>Case</u>	<u>Description</u>
<u>clean</u>	<u>Simulations with aerosol conditions from the days just before the two selected haze episodes start (25 September and 2 October 2013), with daily mean <math>PM_{2.5} &lt; 30 \mu\text{g m}^{-3}</math>.</u>
<u>aged-BC</u>	<u>Simulations on the most polluted days during the two haze episodes (28 September and 5 October 2013), with daily mean <math>PM_{2.5} &gt; 200 \mu\text{g m}^{-3}</math>. The core-shell configuration is assumed for BC and non-BC component mixing. The BC core is assumed as a sphere.</u>
<u>non-BC</u>	<u>The polluted cases but without BC radiative effects by turning off calculations of BC absorption and scattering.</u>
<u>fresh-BC</u>	<u>The polluted cases with fresh BC, in which the BC core is assumed as a sphere but not imbedded in the non-BC shell. The optical properties of the BC core are calculated externally using a Mie theory code. The lensing effect due to aging is not considered in this case.</u>

926

927 **Table 2.** Comparisons between measurements and simulations for aerosol optical properties  
 928 and surface solar radiation during the two haze episodes (EP1/EP2).

<u>Case</u>	<u>SSA</u>	<u>AOD</u>	<u>Max solar radiation flux at surface (W m<sup>-2</sup>)</u>	<u>Accumulated surface solar radiation (MJ m<sup>-2</sup>)</u>
<u>E<sub>MAC-BC</sub> = 2.4</u>	<u>0.83/0.83</u>	<u>3.7/2.1</u>	<u>342/403</u>	<u>10.1/11.5</u>
<u>Aged-BC</u>	<u>0.87/0.87</u>	<u>3.6/2.0</u>	<u>326/402</u>	<u>9.2/11.3</u>
<u>Observations</u>	<u>0.90<sup>a</sup></u>	<u>3.5/2.4<sup>b</sup></u>	<u>480<sup>c</sup>/452</u>	<u>10.6<sup>c</sup>/9.8</u>

929 <sup>a</sup>SSA is based on a recent field campaign conducted in 2015 at Beijing.

930 <sup>b</sup>AOD is based on AERONET measurements at the Beijing site.

931 (<http://aeronet.gsfc.nasa.gov/>).

932 <sup>c</sup>The maximum solar radiation flux and accumulated surface solar radiation were measured at

933 China Meteorological Research Institute, Beijing, China.

934 **Table 3.** RH sensitivity to PBL height changes calculated using the empirical equations by  
 935 Tie et al. (2017). PBL heights are from ceilometer measurements.

	<u>Condition</u>	<u>Mixing Layer Height</u> <u>(meters)</u>	<u>RH</u>	<u>difference in RH (Clean - Hazy)</u>
<b><u>EP1</u></b>	<u>Hazy</u>	<u>395</u>	<u>68%</u>	<u>39%</u>
	<u>Clean</u>	<u>1180</u>	<u>29%</u>	
<b><u>EP2</u></b>	<u>Hazy</u>	<u>370</u>	<u>73%</u>	<u>45%</u>
	<u>Clean</u>	<u>1313</u>	<u>28%</u>	

936

937

Formatted: Left, Space After: 10 pt, Line spacing: Double